Thermal Degradation and Solution Properties of Poly(2,2′-dioxybiphenyl phosphazene)

M. Teresa R. Laguna,[†] M. Pilar Tarazona,[†] Gabino A. Carriedo,[*,‡,§] F. J. García Alonso,[‡] José I. Fidalgo,[‡] and Enrique Saiz[*,†,||]

Departamento de Química Física, Universidad de Alcalá, 28871-Alcalá de Henares, Madrid, Spain; and Departamento de Química Orgánica e Inorgánica, Facultad de Química, Universidad de Oviedo, 33071-Oviedo, Spain

Received April 12, 2002; Revised Manuscript Received June 25, 2002

ABSTRACT: Samples of poly(2,2′-dioxybiphenylphosphazene) were prepared according to procedures previously reported in the literature and submitted to thermal degradation at temperatures between 100 and 200 °C during periods of time ranging from 6 to 250 h. Experimental characterization of the parent polymer and the degraded samples was performed employing DSC and double detector SEC techniques. Values of T_g, molecular weight distributions and averages, molecular dimensions and scaling laws coefficients were thus obtained. THF solutions of this polymer at 25 °C are below Θ conditions although the chain behaves as a random coil. Molecular dimensions of degraded samples are noticeably smaller than those of nondegraded samples of the same molecular weight. Extrapolation to unperturbed conditions gives values of $C_N = 12$ and 7, respectively, for original and degraded samples. Molecular dynamics simulations were also carried out seeking for the conformational properties of the chain which allowed the formulation of a RIS model whose application provides theoretical values of the molecular dimensions in good agreement with experimental results measured for the nondegraded sample.

Introduction

The polyphosphazenes are an important class of inorganic macromolecules which arouse a great interest in modern polymer science from both basic and practical points of view.[1,2] In earlier papers,[3,4] we have reported that the polydichlorophosphazene $[NPCl_2]_n$ reacts with 2,2'-$(HO)C_6H_4-C_6H_4(OH)$ in the presence of K_2CO_3 without cross-linking, allowing the preparation of the new type of phosphazene polymer $[NP(O_2C_{12}H_8)]_n$ (**1**), poly(2,2′-dioxybiphenylphosphazene) (Chart 1), which exhibits a high thermal stability and a high glass transition temperature (T_g on the order of 160 °C).

It has been established that thermal decomposition of polyaryloxyphosphazens occurs in three steps.[5] In the interval 100−250 °C, random cleavage of the polymeric chains gives lower molecular weight polymers. Above 250 °C, depolymerization to cyclic oligomers occurs, and finally, above 400 °C, complex intermolecular coupling reactions take place leading to pyrolitic black residues.

In this work, we investigate the products obtained by thermal degradation of poly(2,2′-dioxybiphenylphosphazene) (**1**) in the lower temperature range. Thus, samples of the parent polymer (**1**) were prepared according to the procedure described elsewhere[4] and submitted to thermal degradation by heating them at temperatures ranging from 150 to 200 °C during periods of time from 6 to 250 h. Four samples, which will be named **1A**, **1B**, **1C**, and **1D**, were thus prepared. Experimental measurements of differential scanning calorimetry, DSC, and size exclusion chromatography, SEC, with dual detection (i.e., simultaneously employing both differential refractive index, DRI, and multiangle light scattering, MALS, detectors) were then performed on the parent polymer and the degraded samples, thus allowing the determination of properties such as T_g, molecular weight distributions and averages, molecular dimensions, and scaling laws parameters. Next, some molecular dynamics, MD, simulations were carried out, seeking the location and relative energies of rotational isomers over skeletal bonds that allows the formulation of a rotational isomeric states model, RIS, for this polymer. Finally, the application of this RIS model produces molecular dimensions which are in good agreement with those experimentally found and permits one to explain some of the most interesting features exhibited by this polymeric chain in solution.

Chart 1

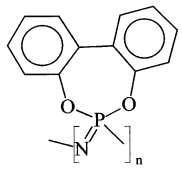

1

Experimental Section

General Remarks. K_2CO_3 was dried at 140 °C prior to use. THF was treated with KOH and distilled twice from Na in the presence of benzophenone. Petroleum ether refers to the fraction having boiling point in the range 60−65 °C. Diphenol $(HO-C_6H_4-C_6H_4-OH)$ was used as purchased (Aldrich).

IR spectra were recorded with a Perkin-Elmer Paragon 1000 spectrometer. Wavenumbers are in cm^{-1}. NMR spectra were recorded on Bruker AC-200 and AC-300 instruments. ^1H and $^{13}C\{^1H\}$ NMR are given in δ relative to TMS. $^{31}P\{^1H\}$ NMR are given in δ relative to external 85% aqueous H_3PO_4. Coupling constants are in Hz. C, H, N analyses were performed with a Perkin-Elmer 240 microanalyzer. T_g values were measured with a Mettler DSC 300 differential scanning calorimeter equipped with a TA 1100 computer. The polymer samples were heated at a rate of 10 °C/min from ambient temperature to 800 °C under constant flow of nitrogen.

* Corresponding authors.
† Universidad de Alcalá.
‡ Universidad de Oviedo.
§ E-mail: gac@sauron.quimica.uniovi.es.
|| Fax: +34918854664. E-mail: enrique.saiz@uah.es.

10.1021/ma020588p CCC: $22.00
Published on Web 08/10/2002

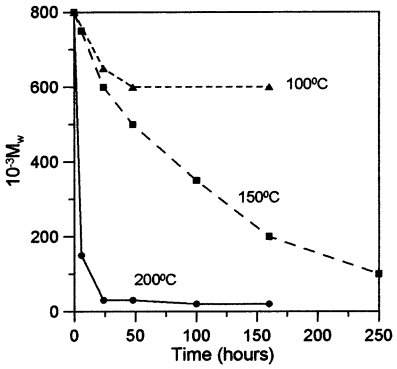

Figure 1. Average M_w, determined by SEC, of the samples obtained after heating polymer **1**.

SEC analyses, aimed to obtain absolute molecular weight distributions, chain dimensions, and scaling laws coefficients, were performed on a dual detector equipment. The concentration detector was a Waters Associates differential refractive index detector, DRI, model 410, and the light-scattering detector, MALS, was a DAWN DSP−F laser photometer from Wyatt Technology Corp. A Model 510 pump, a U6K injector (Waters Associates) and two columns PLgel mixed B (Polymer Laboratories) in series completed the equipment. THF, freshly distilled from sodium and benzophenone, with a 0.1% tetra-*n*-butylammonium bromide was used as eluent. The solvent was filtered through a 0.2 μm Fluoropore membrane and degassed. The flow rate used was 1.0 mL/min. The DAWN photometer was calibrated with spectrometric grade toluene freshly distilled from sodium and benzophenone, and the normalization of the detectors was performed with standard monodisperse polystyrene of low molecular weight that did not show angular dependence on the light-scattering signal. Standard monodisperse polystyrene was also used to determine the interdetector volume using the "spider" plot method.[6]

Synthesis and Thermal Degradation of the Polymers. The parent polymer poly(2,2′-dioxybiphenylphosphazene), $[NP(O_2C_{12}H_8)]_n$ (**1**), was prepared as described in ref 4, employing THF as solvent. The sample thus obtained had $M_w = 8 \times 10^5$ and a bimododal molecular weight distribution as has been observed in previous syntheses.[3,4]

Solid samples of the parent polymer were heated at different temperatures within the range 100−200 °C during periods of time from 6 to 250 h. Figure 1 represents the values of M_w for the products obtained as a function of temperature and time. No loss of mass was observed during the whole process in agreement with the results reported in previous publications.[3,4] However, the thermal degradation produces a decrease in the molecular weight averages of the sample that depends on the combination of time and temperature. The molecular weight distribution of the sample is also modified by the thermal treatment as is illustrated in Figure 2, which represents the SEC chromatograms of the parent polymer and the samples obtained after heating it at 150 °C during different periods of time. These results indicate that lower molecular weight molecules become more abundant as the degradation progresses. C, H, N analysis and spectroscopic properties of the resulting products confirmed the absence of major chemical decomposition with mass loss. Only in the case of the samples heated at 200 °C for long times were there evidences of slight chemical changes (see next paragraph) not accompanied by loss of mass.

Four degraded samples were selected for posterior analysis along with the parent polymer (**1**). They were named **1A**, **1B**, **1C**, and **1D**, and their main characteristics are summarized in Table 1. Thus, columns two and three indicate the combination of temperature and time employed in the degradation. Column four contains the C, H, N analytical data. Finally, T_g and ΔC_p values are collected in the last two columns. All the compounds were white except for sample **1D**, which was brown. Moreover, sample **1D** was not completely soluble in THF. Thus, no further results for this sample are presented.

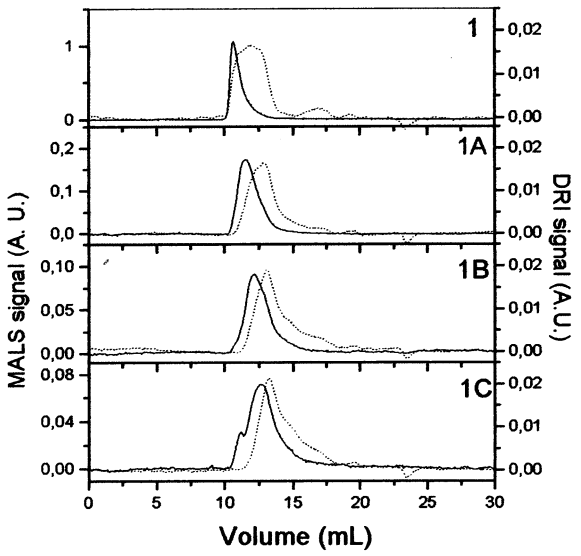

Figure 2. MALS signal at 90° (solid line) and the DRI signal (dot line) for the different samples obtained in a solution of 0.1% tetra-*n*-butylammonium bromide in THF.

Table 1. Preparation, Analytical Data, and DSC Data for the Polymers Studied in This Work

polymer	T (°C)	time (h)	%C, %H, %N (anal. found)	T_g (°C)	ΔC_p (J K^{-1} g^{-1})
1			62.3, 3.0, 6.0	160	0.25
1A	150	100	61.2, 3.0, 5.9	159	0.11
1B	150	160	61.0, 3.2, 5.8	154	0.17
1C	150	250	61.2, 3.1, 5.9	156	0.30
1D	200	24	60.8, 3.8, 6.0	148	0.23

The IR and ^{1}H and ^{13}C NMR spectra of all the polymers were identical with those previously published[3,4] (**1**). High resolution ^{31}P NMR of very concentrated samples of the starting polymer (**1**) showed the expected very strong signal at −5.8 ppm and a very weak triplet at −24.9 ppm ($J_{PP} = 57.1$ Hz) corresponding to the residual $[NPCl_2]$ units. The intensity of this triplet (ca. 0.14%) was in accordance with a Cl content below 0.4% in weight. Other very weak signals at 27 and 8 ppm, could be attributed to the cyclic trimers and tetramers present in **1** as trace impurities (less than 0.05 mol per 100 polymer units $[NP(O_2C_{12}H_8)]$). Therefore, polymer **1** is pure and perfectly linear (not branched). The spectra of the degraded samples showed only one important change in the shape of the strong signal with the appearance of more pronounced shoulders at the lower frequency side of the band, evidencing the increase of the content of lower M_w chains. The content of the $[NPCl_2]$ units and the traces of the cycles remained unchanged. A minor change was the appearance of a very weak doublet at 15.5 ppm ($J_{PP} = 79.4$ Hz) with almost negligible intensity (increasing from nearly 0% in **1A** to 0.8% of the NP units in **1C**).

The DSC curves of **1A** to **1C**, as compared with that of **1** showed that the glass transition temperature, T_g, and the heat capacity increment, ΔC_p, remained almost unchanged, as is shown in the last two columns of Table 1.

SEC Measurements. The basic equation in SEC−MALS is[6]

$$\frac{Kc}{\Delta R_\theta} = \frac{1}{M_w}\left(1 + \frac{16\pi^2}{3\lambda^2}\langle s^2\rangle \sin^2\left(\frac{\theta}{2}\right) + ...\right) \qquad (1)$$

where ΔR_θ is the excess Rayleigh ratio, related to the scattered light intensity of the polymer at angle of observation θ, λ the light wavelength in the solution, $\langle s^2\rangle$ the mean square radius of gyration, and M_w the weight-average molecular weight, and K represents the optical constant that is related to the wavelength in vacuo, λ_0, the solvent refraction index, n,

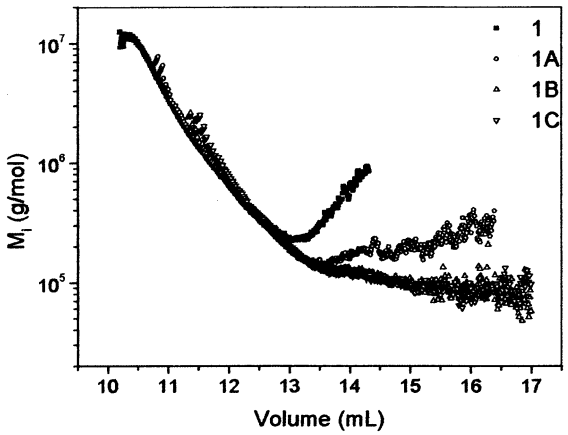

Figure 3. Logarithm of molecular weight vs elution volume.

Avogadros'number, N_A, and refraction index increment, d*n*/d*c* by

$$K = \frac{4\pi^2 n^2}{\lambda_0{}^4 N_A}\left(\frac{dn}{dc}\right)^2 \quad (2)$$

The MALS detector measures simultaneously the excess Rayleigh ratio at different θ angles for each slice *i* of the SEC chromatogram, whereas the differential refractive index detector, DRI, affords the concentration, provided that the d*n*/d*c* value is known. Thus, the use of both detectors allows the calculation of the weight-average molecular weight, the root-mean-square radius of gyration, $\langle s^2\rangle^{1/2}$, and concentration, *c*, for each slice across a sample peak of the size exclusion chromatogram. Assuming that each slice contains molecules of a single molecular weight, or at least a very narrow distribution, absolute calibration curves, i.e., plots of *M* or $\langle s^2\rangle^{1/2}$ vs elution volume, and molecular weight distributions, MWD, can be obtained.

The specific refractive index increment, d*n*/d*c*, for poly(2,2′-dioxybiphenylphosphazene) in THF solution was measured with a Brice-Phoenix differential refractometer at 436 and 546 nm and extrapolated to 632 nm using the Cauchy relationship. A value of 0.153 mL/g was obtained. The calculated masses obtained from the differential refractive index signal and this value of the d*n*/d*c* by the ASTRA software reproduced the injected masses for all of the degraded polymers. Thus, this value of d*n*/d*c* was used throughout all measurements.

Results and Discussion

Molecular Weights. The influence of the heating time on the size exclusion chromatograms is presented in Figure 2 that shows the superposition of the differential refractive index and the 90° light-scattering signals obtained for all the polymer samples in THF with a 0.1% tetra-*n*-butylammonium bromide. The shape of the MALS signal that depends on the product of molecular weight times concentration is different from the DRI signal that depends only on the concentration. Thus, the analysis of the DRI signals shows that the heating favors the displacement of the chromatograms toward higher elution volumes. This fact is a consequence of the degradation of the polymer to progressively lower molecular weights. The manner in which molecular weight changes for the polymer samples provides additional information about the thermal degradation, as will be explained below.

Figure 3 shows the logarithm of the molecular weight plotted vs the elution volume, i.e., absolute molecular weight calibration curves, for the polymers. All the samples, exhibit the same behavior, that is usual in polyphosphazenes,[7−9] the molecular weight decreases as the elution volume increases until an upward curvature appears at low elution volumes. As expected, the curves displace toward higher elution volumes (lower molecular weights) as the heating time increases. Besides, there is a clear superposition of the linear part of the curves, and thus similar molecular weights of the different samples elute at the same volume.

The combined measurements of molecular weight, obtained with the MALS detector, and concentration, obtained with a DRI detector, for each elution volume, allow the determination of the absolute molecular weight distributions for the polymer samples.[6] The values of averaged molecular weights and polydispersity indices, calculated using ASTRA software, are listed in Table 2. The decrease in molecular weight that occurs when either the heating time or temperature increase is evident.

Molecular Dimensions. The analysis of the size of the polymers obtained under different degradation conditions, i.e., combinations of time and temperature, affords further insight into the process of thermal degradation. Figure 4 shows the values of the root-mean-square radius of gyration, $\langle s^2\rangle^{1/2}$, calculated from the angular dependence of the intensity of the scattered light, as a function of the elution volume for samples **1** and **1A**. Data for samples **1B** and **1C** are similar to those of **1A** and are not shown. The *z*-averaged mean square radius of gyration calculated using ASTRA software are shown in Table 2. The root-mean-square radius of gyration provides an excellent representation of the polymer dimensions. As can be seen in the figure, the size of all polymers diminishes as the elution volume increases, in accordance to the SEC separation mechanism, until it reaches a point at which it starts to increase, i.e., a behavior similar to that of the molecular weight. The accuracy of the radius of gyration obtained in the region of high elution volumes (>12 mL) is smaller than that of molecular weight since the size of the polymer should be larger than $\lambda/20$ in order to notice the angular dependence of scattered light. Thus, the error in its values for polymers **1A**, **1B**, and **1C** are greater than for the initial polymer. However these errors do not mask a point of particular interest: There is a clear difference between the size of the initial polymer and the size of the degraded polymers that elute at the same volume. This fact indicates that the degradation causes a change in the shape of the polymer.

Scaling Law. The study of the dependence of radius of gyration on molecular weight, described by the scaling law $\langle s^2\rangle^{1/2} = QM^q$ can give additional information on the structure of the polymers. The values of the power law exponent, *q*, provide a hint about the conditions of the polymeric chain.[10] A value of $q = 0.5$ would indicate a polymer at Θ conditions, values close to 0.6 are obtained for random coil polymers in good solvents, values of $q < 0.5$ are expected for polymers under Θ conditions, and values of $^1/_3$ are obtained for globular (spherical) particles. Figure 5 shows the logarithmic plot of the radius of gyration against molecular weight, for the samples **1** and **1A**. A linear scaling law is obtained only for high values of molecular weight and an upward curvature is found at lower molecular weights. The values of the *q* exponent, for this linear part, obtained by linear regression, and their standard deviations, are presented in the last column of Table 2. The curvature of the scaling law is a consequence of the anomalous

Table 2. Averaged Absolute Molecular Weights, Polydispersity Ratios, Root Mean Square Radii of Gyration, and Scaling Parameters of Polyphosphazenes Studied in This Work

polymer	$10^{-5}M_n$	$10^{-5}M_w$	$10^{-5}M_z$	M_w/M_n	$\langle s^2\rangle_z^{1/2}$ (nm)	q
1	5.6 ± 0.1	17.6 ± 0.8	51 ± 2	3.1 ± 0.1	37 ± 1	0.36 ± 0.01
1A	2.3 ± 0.2	4.9 ± 0.2	16 ± 4	1.9 ± 0.1	16 ± 6	0.38 ± 0.03
1B	1.5 ± 0.1	2.4 ± 0.1	5.6 ± 0.9	1.6 ± 0.1	20 ± 6	0.35 ± 0.02
1C	1.3 ± 0.1	2.0 ± 0.1	4.5 ± 0.5	1.6 ± 0.1	22 ± 6	0.29 ± 0.05

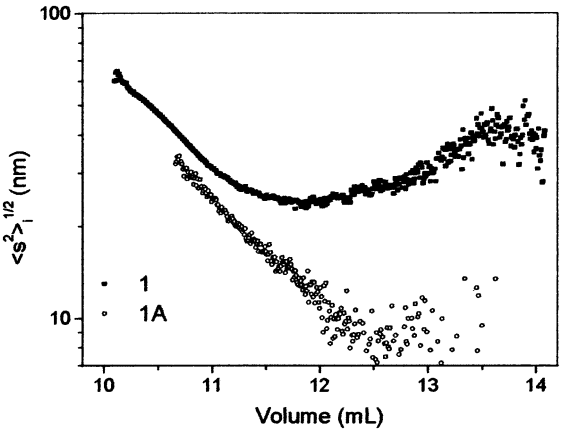

Figure 4. Logarithm of root-mean-squared radius of gyration vs elution volume.

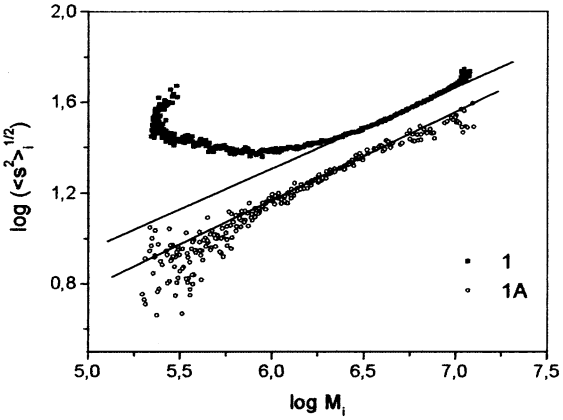

Figure 5. Log−log plot of root-mean-squared radius of gyration vs molecular weight for the polymers in the whole range of molecular weights.

profiles found for molecular weight and radius of gyration, and it is similar to those obtained for other polyphosphazenes[7−9] and other polymers.[11,12] The anomaly is qualitatively explained[11,12] by the existence of a small fraction of very large molecules which are retarded through the SEC columns, due to their size or molecular architecture, and elute at volumes higher than what might be expected by a normal SEC mechanism.

The value of the q parameter for poly(2,2′-dioxybiphenylphosphazene) is 0.36 which might indicate that the polymer chains are below Θ conditions and close to aggregates of globular shape. The values of the q parameter for the degraded polymers **1A**−**1C** present similar values although affected by a much greater error.

The analysis of light-scattering data can also be performed on the basis of the scattering function $P(\theta)$ defined as the ratio of the excess Rayleigh ratio at scattering angles θ and 0

$$P(\theta) = \frac{\Delta R_\theta}{\Delta R_{\theta=0}} \qquad (3)$$

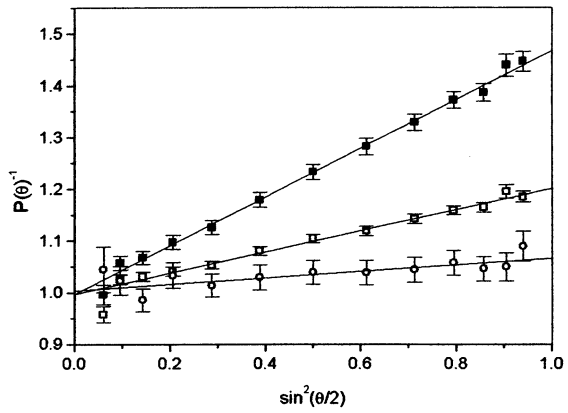

Figure 6. $P(\theta)^{-1}$ as a function of $\sin^2(\theta/2)$ for three different slices: slice at 10.642 mL of polymer **1** (■); slice at 11.208 mL for polymer **1** (□); slice at 11.525 mL for polymer **1A** (○).

Table 3. Elution Volumes, Concentration, Weight Average Molecular Weight, and Root Mean Square Radius of Gyration for Polymers 1 and 1A Obtained for Three Different Slices of the SEC Chromatogram

polymer	V_e (mL)	10^5c (g/mL)	$10^{-6}M_w$	$\langle s^2\rangle_z^{1/2}$ (nm)	D (nm)
1	10.642	1.067 ± 0.007	7.73 ± 0.06	42.1 ± 0.4	109 ± 1
	11.208	1.597 ± 0.007	2.28 ± 0.01	27.5 ± 0.5	71 ± 2
1A	11.525	0.874 ± 0.009	1.32 ± 0.02	16 ± 2	41 ± 5

The reciprocal scattering function, $P(\theta)^{-1}$, can be expanded in terms of the scattering vector **h** as:[13]

$$P(\theta)^{-1} = 1 + \frac{h^2\langle s^2\rangle}{3} - \ldots = 1 + \frac{16\pi^2}{3\lambda^2}\langle s^2\rangle \sin^2\left(\frac{\theta}{2}\right) - \ldots \qquad (4)$$

Thus, it can be calculated from the measured SEC−MALS data (see eq 1) as

$$P(\theta)^{-1} = \frac{Kc}{\Delta R_\theta}\left[\left(\frac{1}{M_w} + 2A_2c + \ldots\right)_{c=0}\right]^{-1} = \frac{Kc}{\Delta R_\theta}M_w \qquad (5)$$

Figure 6 shows the values of $P(\theta)^{-1}$ vs $\sin^2(\theta/2)$ for three different slices. The first two slices are taken from the chromatogram corresponding to polymer **1** at different elution volumes, V_e, whereas the last slice is for polymer **1A** at an elution volume close to the one taken for the second slice of polymer **1** (see Table 3). The values of concentration, molecular weight, and the root-mean-square radius of gyration, obtained for these slices, are also listed in Table 3.

The $P(\theta)$ function for spheres[13] can be calculated as

$$P(\theta) = \left[\frac{3}{u^3}(\sin u - u\cos u)\right]^2 \qquad (6)$$

where $u = (2\pi D/\lambda)\sin(\theta/2)$ and D is the diameter of the sphere, which is related to the radius of gyration by $\langle s^2\rangle = 3D^2/20$.

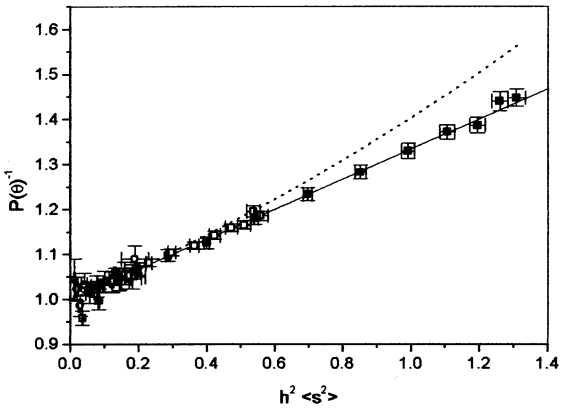

Figure 7. $P(\theta)^{-1}$ as a function of $h^2\langle s^2\rangle$ for three different slices (see legend of Figure 6). Solid line calculated by eq 4. Dotted line calculated by eq 6.

Figure 7 shows the experimental values of $P(\theta)^{-1}$ for the three slices with the fittings according to eq 4 (solid line) and to the spherical shape represented by eq 6, (dotted line) as a function of $h^2\langle s^2\rangle$. As can be seen in Figure 7, the differences between the two models can only be noticed for high values of $h^2\langle s^2\rangle$, i.e., when the molecular weight and the angle of observation are sufficiently large. Thus, the differences between experimental $P(\theta)^{-1}$ and the theoretical sphere model values of the scattering function are only evident for slice 1. This difference suggests that the conformation of the polymer is close to a flexible chain in a very poor solvent, i.e., under Θ conditions.

Unperturbed Dimensions. The values of $\langle s^2\rangle/M$ obtained for these polymers can be used to determine their unperturbed dimensions.[14] The perturbed and unperturbed mean square radius of gyration are related through the chain expansion factor, α:

$$\langle s^2\rangle = \alpha^2\langle s^2\rangle_o \tag{7}$$

and the expression for the expansion coefficient given by the two parameters theory[15,16] is

$$\alpha^2 = (1 + 1.276z - 2.082z^2 + ...) \tag{8}$$

where z is a parameter proportional to $M^{1/2}$. Thus, the values of $\langle s^2\rangle/M$ vs $M^{1/2}$ should fit a polynomial:[17]

$$\frac{\langle s^2\rangle}{M} = \frac{\langle s^2\rangle_o}{M}(1 + AM^{1/2} + BM + ...) \tag{9}$$

with $\langle s^2\rangle_o/M$ as the independent term. Figure 8 shows the experimental values of $\langle s^2\rangle/M$ vs $M^{1/2}$ for polymers **1** and **1A** for which the experimental values of $\langle s^2\rangle$ were determined with more precision. The linear extrapolations of the values at higher molecular weights, which are the ones that follow the scaling law (see Figure 5), yield $\langle s^2\rangle_o/M = (4.19 \pm 0.05) \times 10^{-4}$ and $(2.36 \pm 0.06) \times 10^{-4}$ nm^2 mol g^{-1} for polymers **1** and **1A** respectively. The negative slopes exhibited by the extrapolations (Figure 8) are a straight consequence of the below Θ conditions of the system[15,16]

The characteristic ratio,[14] C_N, can be calculated from the extrapolated value of $\langle s^2\rangle_o$/M as

$$C_N = \frac{\langle r^2\rangle_o}{Nl^2} = \frac{6M_o}{2l^2}\frac{\langle s^2\rangle_o}{M} \tag{10}$$

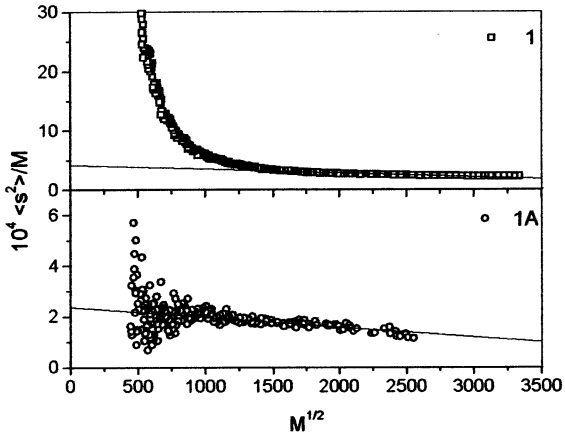

Figure 8. Dependence of experimental values of the ratio between radius of gyration and molecular weight on molecular weight. The solid line shows the extrapolation to unperturbed dimensions.

where N is the number of skeletal bonds, M_o is the molecular weight of the repeating unit, which contains two P−N bonds of length $l = 0.157$ nm, and $\langle r^2\rangle_o$ the unperturbed value of the mean square end to end distance, which for flexible chains is $\langle r^2\rangle_o = 6\langle s^2\rangle_o$. The calculated values of C_N are 12 and 7 for polymers **1** and **1A,** respectively. These values are in good concordance with the different size observed for these polymers through their SEC chromatogram.

Theoretical Calculations

Molecular Dynamics Simulations. (a) Force Field and Molecular Dynamics Software. The modified version of the AMBER force field[18−22] previously employed in the analysis[22] of poly(dichlorophosphazene), PDCPN, was used in the present work. Coulombic interactions were computed as pairwise interactions among partial charges, assigned to every atom of the system by means of the MOPAC-AM1 procedure,[23] employing a distance dependent dielectic constant. Cutoff distances $r_c = 9.6$ and 8 Å were employed respectively for Coulombic and van der Waals interactions, i.e., interactions between atoms i and j were set to zero when their distance r_{ij} is larger than the appropriate r_c. Many different force fields,[22] from very simple to rather sophisticated ones,[24] have been employed up to date to calculate various properties of polyphosphazenes. We prefer to use AMBER, which is relatively simple and easy to use and has been successfully applied to many different kinds of systems.

The DL_POLY package[25] was employed in all the MD simulations performed both in the preparation and thermal equilibration of the samples and in the data collection stages. A time step $\delta = 1$ fs (i.e., 10^{-15} s) was employed for the integration of the equations of motion. The temperature of the systems was kept constant at $T = 300$ K during the data collection by means of a Nose-Hoover thermostat[26] with a relaxation time of 500 fs. However, a homemade routine was incorporated to the package. It acts at regular time intervals, i.e., every 1000 integration steps, randomly selecting one atom of the system and resetting its velocity to the thermal value but with random direction. The effect of this modification is unnoticeable for magnitudes that are averaged over the whole MD trajectory such as temperature, energies, probability distributions, etc. However, it helps the system to overcome potential energy

barriers and therefore speeds up the transition from one minimum to another. Thus, the long time intervals in which the system remains almost unchanged within a local energy minimum are noticeably decreased, and the statistical sampling of the whole conformational space is improved. In fact, the slow rate of conformational changes and the consequent poor statistical sampling is one of the worst difficulties in MD simulations performed at relatively low temperatures.

(b) Molecular Systems. The basic polymeric chain employed in the present calculations was an oligomer containing 45 repeat units of poly(2,2′-dioxybiphenylphosphazene), PDOBPN (i.e., 1080 atoms), whose structure is schematically represented in Chart 1. Rotational angles over skeletal P−N bonds ϕ_{PN} were taken to be 180° for the trans conformation. The data collected during the MD simulations were the rotations over 68 consecutive skeletal bonds in the central part of the chain, i.e., disregarding five repeat units at each extreme in order to avoid end effects.

Three molecular systems were analyzed in the present work. The first one consisted of a single oligomer standing alone in vacuo, and it will be referred to as the oligomer hereafter. The structure of the polymer was first optimized by minimizing its potential energy with respect to all the internal coordinates (i.e., bond lengths, bond angles and rotations). The system was then warmed from 50 to 300 K with temperature increments of 50 K and allowing 500 fs for equilibration a each new temperature. Once the system was equilibrated at the working temperature, $T = 300$ K, the data collection stage was initiated. It consisted in a MD trajectory of 3×10^6 integration steps (i.e., 3 ns) during which the data of interest were recorded every 100 integration steps.

The second molecular system was intended to simulate a bulk amorphous sample of PDOBPN and contains two oligomers packed into a cubic box having periodic boundary conditions, a side length $L = 30.4$ Å, and therefore a density of ca. 1 g cm^{-3}. This system will be referred to as bulk. The system was first built into a much larger box with a side length roughly twice the final desired value in order to avoid interpenetration among segments of the polymer that would render difficult and unreliable any conceivable scheme for energy minimization. A MD simulation under *NVT* conditions at $T = 500$ K was then started, and the size of the box, and consequently the volume of the system, was decreased with small increments, leaving relaxation times of 500 fs for the system to equilibrate at each new volume. Once the final volume was achieved, several annealing cycles were applied to the sample consisting in heating and cooling the system between 50 and 500 K with temperature increments of 50 K and equilibration times of 500 fs at every new temperature. Finally, the system was warmed from 50 K to the working temperature of 300 K under *NpT* conditions again with temperature increments of 50 K and equilibration times of 500 fs. The data collection stage consisted in 5×10^6 integration steps (i.e., a time span of 5 ns) performed under *NpT* conditions while recording the data of interest every 100 steps.

The third system was a solution containing one oligomer and 100 molecules of THF packed into a PBC box with $L = 29.8$ Å and density of 1 g cm^{-3}. This system will be named solution. The preparation of the sample and the data collection stage were identical with those of the bulk system.

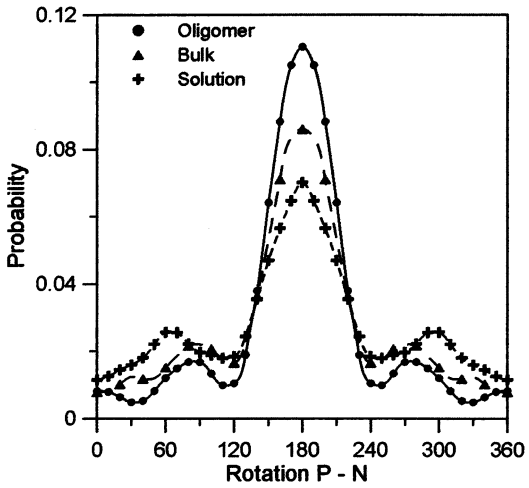

Figure 9. Probability distribution for rotations over the skeletal bonds assuming that each bond is independent of its neighbors. Values were computed at 300 K and averaged over the 68 rotations on the central part of the polymeric chain.

(c) Results. The raw results of the MD simulations consisted in rather huge sets of values of 68 rotational angles over the skeletal P−N bonds. The simplest way of analyzing those results is to count how many times each of those rotations adopted a given value, with a determined tolerance, during the MD trajectory (for instance, how many times the studied angle lies within the interval $10 \pm 5°$). The result divided by the total number of analyzed conformations gives the probability distribution for these rotations assuming that the rotation of each bond is independent of its neighbors. The results thus obtained, averaged over the 68 rotations studied for each polymeric chain and over symmetrical positions in order to eliminate small distortions of the raw data, are represented in Figure 9. As it is apparent from Figure 9, the trans (i.e., $\phi \approx 180°$) orientation is, by far, the preferred orientation for the skeletal bonds of the PDOBPN chain as it happens in other polyphosphazenes such as PDCPN.[22] However, unlike PDCPN, the cis orientation (i.e., $\phi \approx 0°$) has a very low incidence within the chain of PDOBPN that presents instead conformations close to the staggered gauche orientations $g^{\pm}$ (i.e., $\phi \approx \pm 60°$) that are typical of polymers having carbon backbones such as polystyrene. Of course, this behavior is a direct consequence of the structure of the dioxybiphenyl group in the PDOBPN chain as will be explained below.

However, the assumption of independent rotations, although useful for a qualitative determination of the overall preferences of the skeletal bonds, is not a good approximation for the description of a polymeric chain.[14,27−29] A much more detailed picture can be obtained by a simultaneous analysis of pairs of consecutive bonds. The distribution of a priori probabilities for the two different pairs of consecutive bonds, i.e., P−N−P and N−P−N pairs, of the three systems studied were computed in the same way than the independent probabilities, namely counting how many times the rotations over a given pair of bonds adopted a determined pair of values with a tolerance of ±5°. The results indicate that the maxima of probability correspond roughly to the nine combinations of the three orientations (i.e., t, $g^{\pm}$) allowed to each independent bond. The highest probability corresponds to the tt orientation followed by the four combinations in which one bond is in t and the other

one either in g^+ or g^+ (i.e., $tg^{\pm}$ and $g^{\pm}t$) and then by the two orientations having both angles in gauche states of the same sign (i.e $g^{\pm}g^{\pm}$) while the combinations of two gauche states of opposite sign (i.e., $g^{\pm}g^{\mp}$) have very little incidence.

A more quantitative analysis can be performed by integrating the area under the probability peaks within a given distance $\Delta\phi$ from the maxima. The results thus obtained represent the probability for the allowed conformations of each pair of bonds ϕ_{i-1},ϕ_i and are customarily written as a matrix whose rows are associated with the rotational state of bond $i - 1$ and whose columns represent the states of bond i. Integration of the probabilities taking $\Delta\phi = 40°$ gives the following results, normalized to unity, for the two pairs of bonds of the solution with the rotational isomers in the order g^+, t, g^-:

solution:

$$\mathbf{P}_{PNP} = \begin{bmatrix} 0.032 & 0.136 & 0.016 \\ 0.136 & 0.360 & 0.136 \\ 0.016 & 0.136 & 0.032 \end{bmatrix}$$

$$\mathbf{P}_{NPN} = \begin{bmatrix} 0.056 & 0.135 & 0.010 \\ 0.135 & 0.328 & 0.135 \\ 0.010 & 0.135 & 0.056 \end{bmatrix} \quad (11)$$

The results obtained for the other two systems are

bulk:

$$\mathbf{P}_{PNP} = \begin{bmatrix} 0.006 & 0.128 & 0.017 \\ 0.128 & 0.442 & 0.128 \\ 0.017 & 0.128 & 0.006 \end{bmatrix}$$

$$\mathbf{P}_{NPN} = \begin{bmatrix} 0.035 & 0.140 & 0.000 \\ 0.140 & 0.370 & 0.140 \\ 0.000 & 0.140 & 0.035 \end{bmatrix} \quad (12)$$

oligomer:

$$\mathbf{P}_{PNP} = \begin{bmatrix} 0.001 & 0.046 & 0.046 \\ 0.046 & 0.723 & 0.046 \\ 0.046 & 0.046 & 0.001 \end{bmatrix}$$

$$\mathbf{P}_{NPN} = \begin{bmatrix} 0.005 & 0.110 & 0.000 \\ 0.110 & 0.550 & 0.110 \\ 0.000 & 0.110 & 0.005 \end{bmatrix} \quad (13)$$

Averaging the values of the rotational angles for the same area under the peaks employed to compute the probabilities provides the mean location of the rotational isomers as: $\phi_t \approx 180°$, $\phi_{g\pm} \approx \pm 60°$ for all the systems.

The three systems present the same main features, namely a strong preference for tt conformations and a small incidence of two consecutive bonds in gauche states. To understand these conformational preferences, it is important to realize that, despite what Chart 1 may suggest, the dioxybiphenyl group is not planar. On the contrary, in the most stable conformation, the planes containing each one of the two phenoxy groups form a dihedral angle of ca. 54° and the P atom is placed over the bisectrix of that angle, as it is shown in Figure 10 that represents a segment of three repeating units in the all-trans conformation and indicates that all the rings located on the same side of the skeleton are tilted

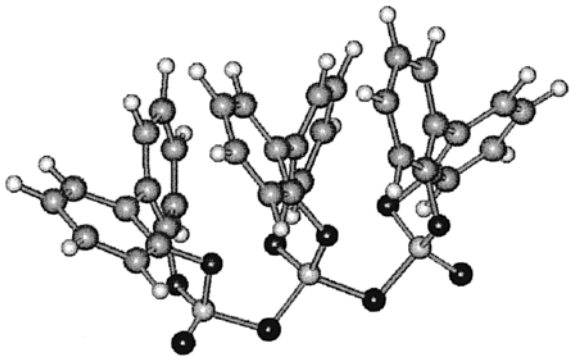

Figure 10. Three repeating units of the PDOBPN chain in the all-trans conformation. The planes containing the oxyphenyl groups of each repeating unit make an angle of ca. 54°, and the P atom is placed roughly in the bisectrix of that angle. All the rings located above the plane of the skeleton are tilted to the same side (to the left in this figure), while rings placed below the skeleton are tilted to the contrary side.

in the same direction. There are two equivalent arrangements, either the one shown in Figure 10 with the rings above the skeleton tilted to the left and those below rotated to the right or the other one in which the directions of rotations are reversed. Obviously, both arrangements are equivalent and they appear roughly with the same frequency along the MD simulation although they cannot interconvert from one to another because the rotation over the Phe−Phe bond would produce severe overlapping of groups attached to neighbor units. However, they can reverse the orientation when one of the skeletal bonds is in gauche conformation. But, the most important feature illustrated by Figure 10 is that all the groups are separated by rather large distances so that their interactions are attractive and this conformation is the most stable one. One last characteristic of the chain that may be appreciated in Figure 10 is that the skeletal backbone does not propagate along a straight line when it is in the all-trans conformation but curves over itself due to the difference of ca. 10° in the skeletal bond angles ($\theta_{PNP} \approx 131°$, $\theta_{NPN} \approx 121°$) producing, as a consequence, that the equivalent phenyl rings are not parallel to each other but diverge like the radius of a wheel.

Unlike the all-trans conformation, the trans, cis conformation, i.e., $\phi_i = 180$, $\phi_{i+1} = 0$, which is represented in Figure 11, places the skeletal N atom at distances (indicated by arrows in the figure) of ca. 2 Å from the P, and the two O atoms of the next unit, thus producing strong repulsions that preclude the existence of this conformation. These repulsions may be relieved through rotation of the skeletal bond toward the gauche orientation ($\phi \approx \pm 60°$) as is represented in Figure 12b. For this reason, the PDOBPN chain prefers gauche rather than cis conformations, while other polyphosphazenees such as PDCPN exhibit cis instead of gauche conformations.[22]

Figure 12 represents the four non equivalent orientations for the pair of bonds P−N−P. Part c of this Figure shows that the most important interactions for a pair of gauche states of the same sign $g^{\pm}g^{\pm}$, is the N···O. On the same way, part d indicates that N···N is the most important interaction for combinations of two gauche states of opposite sign $g^{\pm}g^{\mp}$. Figure 13 represents the same kind of conformations for the skeletal pairs of bonds N−P−N and shows that P···O are the important interactions in $g^{\pm}g^{\pm}$ conformations (part c), while

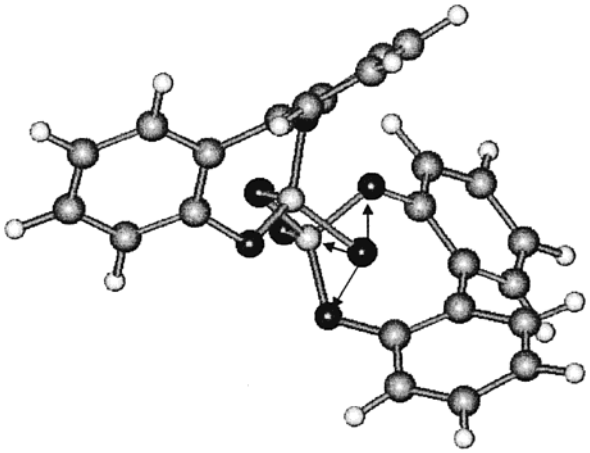

Figure 11. Conformation trans, cis for a pair of P−N−P skeletal bonds of the PDOBPN chain. The skeletal N atom is placed at distances (indicate by arrows in Figure) of ca. 2 Å from the P atom, and the two O atoms of the next unit; thus, it produces strong repulsions that preclude the existence of this conformation.

P···P is the relevant interaction for $g^{\pm}g^{\mp}$ represented in part d.

Conformational Model. The probability matrices $\mathbf{P}_{PNP}$ and $\mathbf{P}_{NPN}$ indicated in eqs 11−13 can be transformed into statistical weight matrixes[14,27−29] written as a function of Boltzmann factors of the first and second-order interactions illustrated in Figures 12 and 13. Thus, taking the tt conformation as reference and writing the isomers in the order g^+, t, and g^-, the statistical weight matrices for the two kinds of pairs of skeletal bonds are

$$\mathbf{U}_{PNP} = \begin{bmatrix} \sigma\gamma & 1 & \sigma\omega \\ \sigma & 1 & \sigma \\ \sigma\omega & 1 & \sigma\gamma \end{bmatrix} \quad \mathbf{U}_{NPN} = \begin{bmatrix} \sigma\gamma' & 1 & \sigma\omega' \\ \sigma & 1 & \sigma \\ \sigma\omega' & 1 & \sigma\gamma' \end{bmatrix} \quad (14)$$

where each statistical weight factor represents a Boltzmann exponential of its corresponding interaction energy. Thus, for instance $\sigma = \exp(-E_\sigma/RT)$. The meaning of these interactions is summarized in Table 4.

The conformational partition function for a chain containing x repeat units may by computed as a serial product of these statistical weight matrices as[14,27−29]:

$$Z = [1 \;\; 0 \;\; 0](\mathbf{U}_{PNP}\mathbf{U}_{NPN})^{x-1}\begin{bmatrix}1\\1\\1\end{bmatrix} \quad (15)$$

The a priori probability for a pair of P−N−P bonds, placed in the center of a chain containing $2x + 2$ repeat units, being in conformational state ij may be computed as

$$p_{ij}(\mathrm{PNP}) = Z^{-1}[1 \;\; 0 \;\; 0](\mathbf{U}_{PNP}\mathbf{U}_{NPN})^{x}\mathbf{U}_{PNP}{}^{0}\mathbf{U}_{NPN}(\mathbf{U}_{PNP}\mathbf{U}_{NPN})^{x}\begin{bmatrix}1\\1\\1\end{bmatrix} \quad (16)$$

where U^0_{PNP} is obtained by replacing all the elements of the U_{PNP} matrix by zero except element ij which is left unchanged. The same procedure may be applied to compute the probabilities p_{ij}(NPN) with $\mathbf{U}_{PNP}\mathbf{U}^0_{NPN}$ instead of $\mathbf{U}^0_{PNP}\mathbf{U}_{NPN}$ in the central part of eq 16. The calculation can be repeated with different values of the conformational energies seeking for the best fit to the probabilities obtained from the MD simulation. Table 5 summarizes the values of conformational energies for the three systems studied that reproduce the probabilities indicated in eqs 11−13.

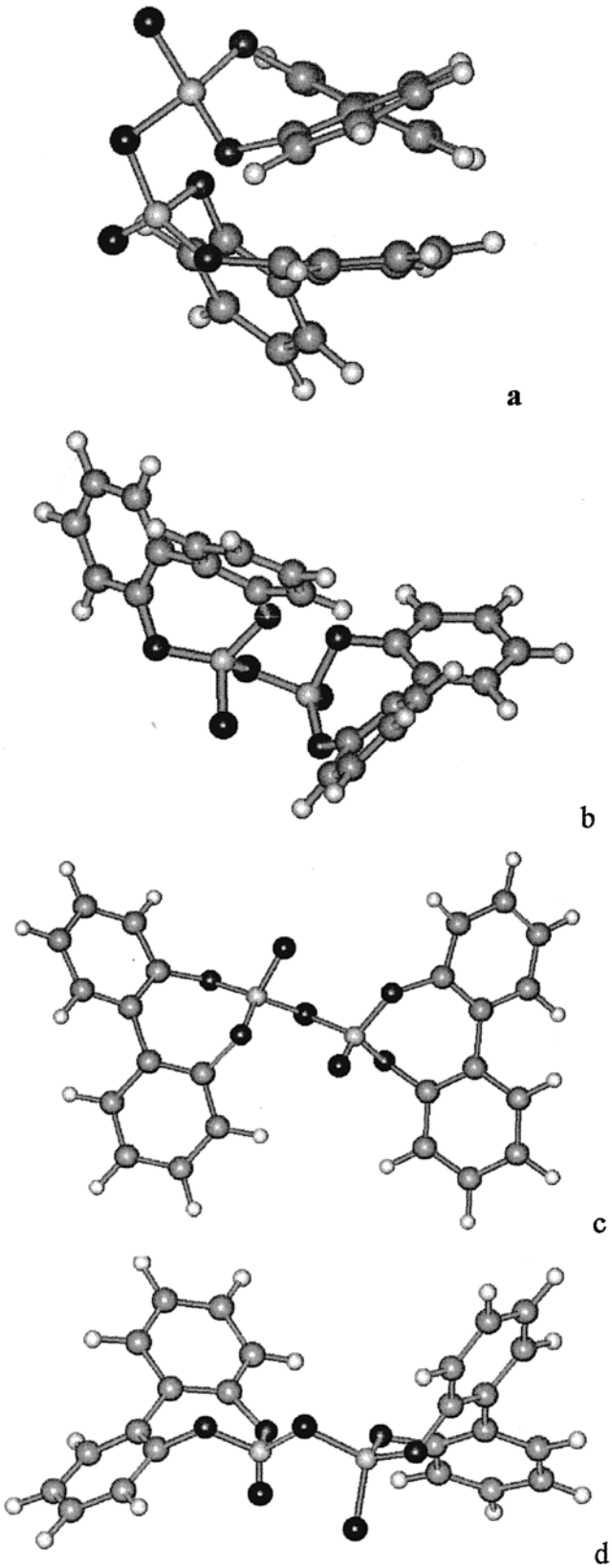

Figure 12. Allowed conformations for a pair of P−N−P skeletal bonds of the PDOBPN chain: (a) tt; (b) tg (equivalent to tg^-, gt, and g^-t); (c) $g^{\pm}g^{\pm}$; (d) $g^{\pm}g^{\mp}$.

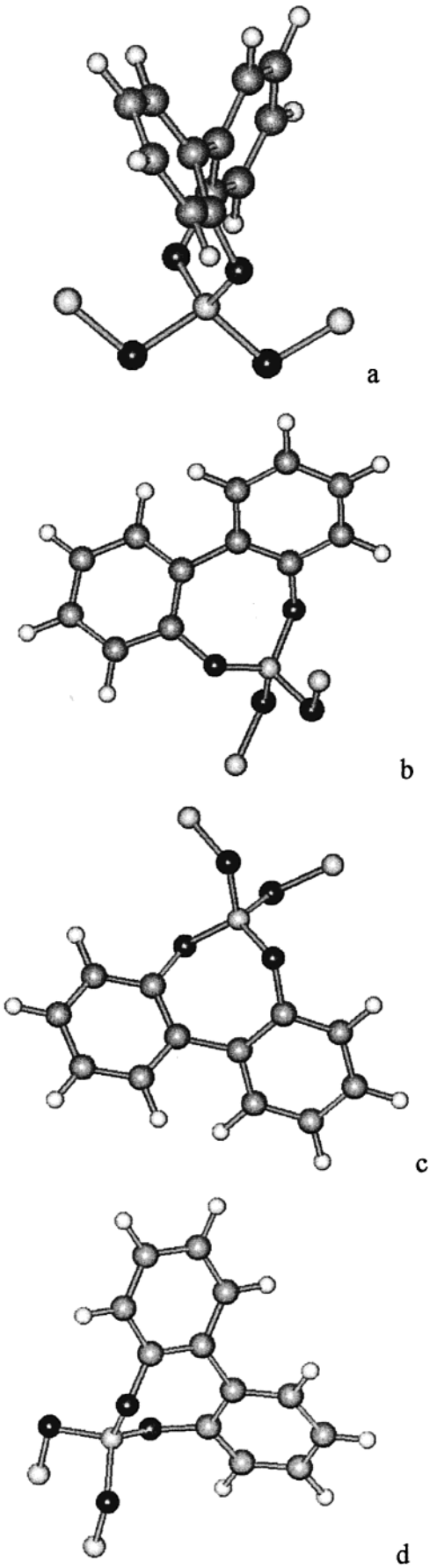

Figure 13. Same as Figure 12 for the skeletal pair of bonds N−P−N.

Table 4. Statistical Weights, Normalized to Trans−Trans Conformation, for the U_{PNP} and U_{NPN} Matrices Representing the Conformational States Allowed to P−N−P and N−P−N Pairs of Skeletal Bonds in PDOBPN[a]

statistical weight	energy	conformation	interaction	order
σ	E_σ	$g^\pm$ in any bond	N···O and N···P	first
γ	E_γ	$g^\pm g^\pm$ in PNP	N···O	second
ω	E_ω	$g^\pm g^\mp$ in PNP	N···N	second
γ'	$E_{\gamma'}$	$g^\pm g^\pm$ in NPN	P···O	second
ω'	$E_{\omega'}$	$g^\pm g^\mp$ in NPN	P···P	second

[a] See Figures 12 and 13.

Table 5. Values of Conformational Energies, in kcal mol^{-1}, for the Three Systems Studied That Reproduce the a Priori Probabilities Computed from MD Simulations and Represented in Eqs 11−13

	molecular system		
energy	solution	bulk	oligomer
E_σ	0.41	0.48	1.46
E_γ	0.37	1.32	0.86
E_ω	0.78	0.61	−1.62
$E_{\gamma'}$	−0.07	0.10	0.69
$E_{\omega'}$	0.94	3.10	4.36

Unperturbed dimensions of the polymeric chain can be computed with the statistical weight matrices according to standard procedures of the matrix multiplication scheme.[14,27−29] Calculations were performed at $T = 300$ K with the conformational energies summarized in Table 5 and the rotational isomers placed at $\phi_t = 180°$, $\phi_{g\pm} = \pm 60°$ for all the systems. Polymeric chains containing up to $N = 400$ skeletal bonds were generated, their mean squared end-to-end distance $\langle r^2 \rangle$ was computed and transformed into the dimensionless characteristic ratio $C_N = \langle r^2 \rangle / Nl^2$ with $l = 1.57$ Å being the length of the skeletal P−N bond. The results are shown in Figure 14 which indicates that the three systems behave as random coils with values of C_N increasing with increasing values of N and leveling of to an asymptotic limit for relatively short chains with ca. $N \approx 100$ skeletal bonds. The asymptotic limits for very long chains, i.e., $N \rightarrow \infty$ are $C_\infty = 7.9$, 13.2, and 11.1, respectively, for the oligomer, bulk, and solution systems.

It may seem surprising that the oligomer, which according to Figure 9 and eqs 11−13 contains the highest proportion of trans states in the chain, produces the smallest molecular dimensions as is shown in Figure 14. This result is a consequence of two conformational characteristics of the chain, namely that the all-trans conformation curves over itself due to the difference in skeletal bond angles and that gauche instead of cis is the second allowed state besides trans, and it can be easily understood by computing the average length of trans sequences in the polymeric chains of the three systems. According to the $\mathbf{P}_{PNP}$ matrix for the solution given in eq 11, the probability for the P−N bond in the P−N−P pair being trans is $p_t = 0.632$ (sum of the elements in the second row of the matrix), and the probability of both bonds being in tt is 0.360 (element 2,2 of the matrix). Therefore, the probability of replication for trans, i.e., the probability of a trans state being followed by another trans is $p_r = p_{tt}/p_t = 0.570$ and the probability of inversion, i.e., the probability of a trans state being followed by either g^+ or g^- is $1 - p_r$. The same calculation for the $\mathbf{P}_{NPN}$ matrix of the solution gives $p_r = 0.548$. A sequence of n_t bonds in the all-trans

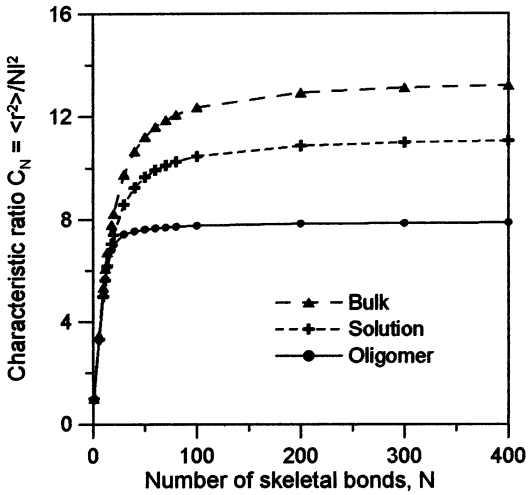

Figure 14. Characteristic ratios of the three systems studied as a function of the number of skeletal bonds contained in the chain. Calculations were performed at $T = 300$ K with the statistical weight matrices represented in eq 14, the energies summarized in Table 5. and the rotational isomers placed at 180, ±60°.

conformation would require $n_t - 1$ replications and one inversion and therefore has a probability of $p_r^{n-1}(1 - p_r)$. The average value of n_t can then be obtained as

$$\langle n_t \rangle = (1 - p_r)\sum_{i=1}^{\infty} i(p_r)^{i-1} = \frac{1}{1 - p_r} \qquad (17)$$

The value of p_r can be taken as the average among the two values obtained from P−N−P and N−P−N matrixes[30] that amounts to 0.559, 0.601, and 0.801 respectively for the solution, bulk, and oligomer. Substitution of these values into eq 17 yields $\langle n_t \rangle \approx 2.3$, 2.5, and 5.0 for these systems.

Thus, the structure of the PDOBPN polymeric chain either in THF solution or in the bulk consists of relatively short sequences of t conformations, i.e., 2 or 3 bonds, so that the curvature of this arrangement is almost negligible, disrupted by $g^{\pm}$ conformations, with almost negligible incidence of consecutive pairs of bonds in any combination of gauche states. This produces a helix structure, although it is distorted mainly because two gauche states with different orientations are allowed. Nevertheless, it has a well-defined direction of propagation and produces large molecular dimensions. On the other hand, trans sequences on the oligomer are longer (roughly twice than in the other systems), the curvature is more important, and the helical structure is much more distorted so that the direction of propagation is not so well-defined and consequently produces much smaller molecular dimensions.

Among the three systems studied in this work, the oligomer has no equivalence to any experimental situation, although its analysis is important for comparative purposes. Quantitative differences observed among the results obtained for the three systems are due to intramolecular long-range interactions,[31] i.e., interactions among groups separated by more than two consecutive skeletal bonds that may be placed at short distances in compact conformations.[14,27−29] These interactions are present in the oligomer and, in average, are repulsive because the groups involved are quite huge while they are attractive in other polyphosphazenes such as PDCPN where the side groups are very small.[22] For this reason, the preference for tt conformations that minimize those interactions is very high in the oligomer. In bulk, the system is in the unperturbed state, or Θ condition, which amounts to saying that the long-range interactions are exactly compensated for by intermolecular interactions with other chains (or segments of chains) contained in the periodic box. In this case, removal of long-range interactions means to increase the probability of gauche orientations (or decrease the probability of trans) since some repulsions produced in the compact conformations are removed. Finally, in solution, the long-range interactions are replaced by polymer−solvent interactions that may be stronger, equal or weaker than the polymer−polymer interactions, respectively for good, Θ, and poor solvents. In this case, the results obtained for solution and bulk are not identical, which means that THF is not a Θ solvent for this polymer. The differences are not large, but the unperturbed dimensions computed for bulk are higher than those obtained for the solution, which indicates that the solution is below Θ conditions.

Polyphosphazenes are frequently compared with polysiloxanes seeking for similarities and differences among the two kinds of inorganic skeleton. In this sense, PDOBPN could be compared with poly(diphenyl siloxane), PDPS, and it is surprising that the characteristic ratio calculated for this last polymer[32] is roughly five times larger than the value obtained in this work for PDOBPN. Thus, even if the side group is much more rigid in PDOBPN than in PDPS, the polymeric skeleton is stiffer in PDPS.

The values of C_∞ computed with the theoretical scheme presented above are in excellent agreement with the experimental results measured for the nondegraded sample. However, they severely overestimate the experimental results of the degraded samples. We cannot present a fully satisfactory explanation for this decrease of the molecular dimensions in terms of the structural properties of the polymeric chains. In fact, the lower values of characteristic ratios might be explained by either one or a combination of the following effects: (a) very short chains; (b) the presence of anomalous units within the chain; (c) branching of the polymeric chains.

The first possibility can be easily ruled out since Figure 14 indicates that the value of C_N reaches the asymptotic limit C_∞ for very long chains at $N \approx 100$, i.e., $M \approx 11\,000$, which according to the results summarized in Table 2 is much smaller than that for the samples measured in this work.

Anomalous units might be produced within the chain by assuming that the thermal degradation breaks down some O−P bonds, thus creating some cleaved units in which the side groups are not a cycle and therefore exhibit higher conformational mobility. Exploratory calculations indicate that an overall content of ca. 10% of such cleaved units would be required to account for the experimental difference in the values of C_∞. However, the NMR spectra of degraded samples showed no evidence of such cleaved units and furthermore, previous analysis[5] indicate that temperatures of ca. 400 °C, i.e., 150 °C above the highest temperature employed in the present work, would be required to break down this kind of bonds.

Therefore, since the starting polymer is linear (see experimental part and the agreement between its dimensions and those computed for perfectly linear chains), the remaining possible explanation is branching

of the polymeric chains produced during the thermal degradation, probably at the residual ($NPCl_2$) units of the parent polymer. However, no experimental evidence of this branching could be detected in the NMR spectra of the degraded samples (see Experimental Section). But, on the other hand, it is also true that a few very long branches might reduce the dimensions significantly, even though the number of branch points was so small that it might escape detection in NMR.

Conclusions

Thermal degradation of poly(2,2′-dioxybiphenylphosphazene) (**1**) at temperatures from 100 to 200 °C during periods of time up to 250 h takes place with neither loss of mass nor a noticeable change in the chemical structure of the polymer. The analysis of SEC chromatograms obtained with dual detection equipment in THF solutions at 25 °C indicates that the polymer is below Θ conditions although not far from them. Molecular dimensions of degraded samples are always smaller than those of nondegraded samples of the same molecular weight.[33] Extrapolation to Θ conditions gives values of the characteristic ratio of molecular dimensions $C_N = 12$ and 7 respectively for original and degraded samples. A detailed and fully satisfactory molecular explanation for this decrease of dimensions is not available at this moment.

Molecular dynamics simulations performed on systems containing segments of PDOBPN indicate that the skeletal bonds on this chain have three allowed conformations, namely trans and the two gauche, with a strong preference for trans. The chain exhibit a distorted helical structure. Characteristic ratios computed in THF solutions ($C_N = 11.1$) are smaller than those obtained in the bulk ($C_N = 13.2$) which confirms that the THF solution is below Θ conditions.

Acknowledgment. The financial support provided by the DGICYT through Projects PB97-0778, PB97-1276, and BQU2001-1158 is gratefully acknowledged.

References and Notes

(1) Mark, J. E.; Allcock, H. R.; West, R. *Inorganic Polymers*; Prentice Hall: Englewood Cliffs, NJ, 1992.
(2) De Jaeger, R.; Gleria, M. *Prog. Polym. Sci.* **1998**, *23*, 179.
(3) Carriedo, G. A.; Fernández-Catuxo, L.; García Alonso, F. J.; Gómez Elipe, P.; González, P. A. *Macromolecules* **1996**, *29*, 5320.
(4) Carriedo, G. A.; García Alonso, F. J.; Gómez Elipe, P.; González, P. A.; Marco, C.; Gómez, M. A.; Ellis, G. *J. Appl. Polym. Sci.* **2000**, *77*, 568.
(5) Allcock, H. R.; McDonnell, G. S.; Riding, G. H.; Manners, I. *Chem. Mater.* **1990**, *2*, 425.
(6) Wyatt, P. J. *Anal. Chim. Acta* **1993**, *272*, 1.
(7) Búrdalo, J.; Tarazona, M. P.; Carriedo, G. A.; García Alonso, F. J.; González, P. A. *Polymer* **1999**, *40*, 4251.
(8) Carriedo, G. A.; García Alonso, F. J.; González, P. A.; García Alvarez, J. L.; Tarazona, M. P.; Rodriguez, M. T.; Saiz, E.; Vazquez, J. T.; Padrón, J. I. *Macromolecules* **2000**, *35*, 3671.
(9) Laguna, M. T. R.; Saiz, E.; Tarazona, M. P. *Polymer* **2000** *41*, 7993.
(10) De Gennes, P. G. *Scaling Concepts in Polymer Physics*; Cornell University Press: Ithaca, NY, 1979.
(11) Percec, V.; Ahn, C. H.; Cho, W. D.; Jamieson, A. M.; Kim, J.; Leman, T.; Schmidt, M.; Gerle, M.; Möller, M.; Prokhorova, S. A.; Sheiko, S. S.; Cheng, S. Z. D.; Zhang, A.; Ungar, G.; Yeardley, D. J. P. *J. Am. Chem. Soc.* **1998**, *120*, 8619.
(12) Gerle, M.; Fischer, K.; Roos, S.; Müller, A. H. E.; Schmidt, M. *Macromolecules* **1999**, *32*, 2629.
(13) Huglin, M. B. Ed. *Light Scattering from Polymer Solutions*; Academic Press: London, 1972; Chapter 7.
(14) Flory, P. J. *Statistical Mechanics of Chain Molecules*; Wiley: New York, 1969.
(15) Yamakawa, H. *Modern Theory of Polymer Solution*; Harper and Row: New York, 1971.
(16) Yamakawa, H. *Macromolecules* **1993**, *26*, 5061.
(17) Laguna, M. T. R.; Tarazona, M. P. *Polymer* **2001** *42*, 1751−1756.
(18) Weiner, S. J.; Kollman, P. A.; Case, D. A.; Singh, U. C.; Ghio, C.; Alagona, G.; Profeta, S.; Weiner, P. *J. Am. Chem. Soc.* **1984**, *106*, 765.
(19) Weiner, S. J.; Kollman, P. A.; Nguyen, D. T.; Case, D. A. *J. Comput. Chem.* **1986**, *7*, 230.
(20) Homans, S. W. *Biochemistry* **1990**, *29*, 9110.
(21) Cornell, W. D.; Cieplak, P.; Bayly, C. L.; Gould, I. R.; Merz, K, M.; Ferguson, D. M.; Spellmeyer, D. C.; Fox, T.; Caldwell, J. W.; Kollman, P. A. *J. Am. Chem. Soc.* **1995**, *117*, 5179.
(22) Tarazona, M. P.; Saiz, E. *Polymer* **2000**, *41*, 3337.
(23) MOPAC, *Quantum Chemistry Program Exchange*, Department of Chemistry, Indiana University, Bloomington, IN.
(24) Sun, H.; Ren, P.; Fried, R. *Comput. Theor. Polym. Sci.*, **1998**, *8*, 229.
(25) Forester, T. R.; Smith, W. *DL_POLY* (Ver. 2.10), Daresbury Laboratory, Daresbury, Warrington WA4 4AD, England.
(26) Allen, M. P.; Tildesley, D. J. *Computer Simulation of Liquids*; Clarendon: Oxford, England, 1987.
(27) Flory, P. J. *Macromolecules* **1974**, *7*, 381.
(28) Riande, E.; Saiz, E. *Dipole Moments and Birefringence of Polymers*; Prentice-Hall: Englewood Cliffs, NJ, 1992.
(29) Mattice, W. L.; Suter, U. W. *Conformational Theory of Large Molecules*; Wiley: New York, 1994.
(30) A more precise calculation, taking into account the two different values of p_r produced by the two distinct matrices, can be performed. However, the results thus obtained are almost identical with those computed with the average, which is a more intuitive procedure.
(31) From a formal point of view, the statistical model employed in this work to compute molecular dimensions, i.e., eqs 14−16 together with Tables 3 and 4, contains only short range energies. However, they were obtained through the analysis of conformations of a relatively long chain in which long-range interactions are present. Consequently, their adjusted values, given in Table 4, are produced by both short and long-range interactions. See ref 22.
(32) Patil, R. D.; Mark, J. E. *Comput. Theor. Polym. Sci.* **2000**, *10*, 189.
(33) The ratio $r_i = \langle s^2\rangle_i^{1/2}/M_i$ for a monodisperse slice *decreases* from sample **1** to sample **1C.** However, according to the data shown in Table 2, the ratio $r_z = \langle s^2\rangle_z^{1/2}/M_z$ *increases* from sample **1** to sample **1C.** The reason is that $\langle s^2\rangle_i^{1/2}$ scales with M^q with $q \approx 0.3$, and therefore, r_i decreases with increasing M_i. Thus, the sample with highest M_z (sample **1**) has the lowest value of r_z.

MA020588P